ELSEVIER

Contents lists available at ScienceDirect

Applied Ocean Research

journal homepage: www.elsevier.com/locate/apor





Data-driven modeling of Bay-Ocean wave spectra at bridge-tunnel crossing of Chesapeake Bay, USA

Nan Wang a, Qin Chen b,*, Ling Zhu a

- ^a Department of Civil and Environmental Engineering, Northeastern University, 360 Huntington Avenue, Boston, MA 02115, USA
- ^b Department of Civil and Environmental Engineering, and Department of Marine and Environmental Sciences, Northeastern University, 360 Huntington Avenue, Boston, MA 02115, USA

ARTICLEINFO

Keywords: Chesapeake Bay Bridge-Tunnel Artificial neural network Spectral wave modeling Wave hindcast Wave spectra Deep learning

ABSTRACT

The Chesapeake Bay Bridge-Tunnel (CBBT) was designed in the early 1960s and first opened on April 15, 1964. It is a 28.3-km bridge-tunnel system that crosses the mouth of Chesapeake Bay. Because there is a lack of reliable long-term observations of surface waves near the Chesapeake Bay entrance, accurate forecasts and hindcasts of wave conditions are essential for maintaining and expanding the bridge-tunnel infrastructure. To estimate wave parameters and energy spectra near the CBBT, novel composite data-driven models were developed using the wind, water level, and offshore wave data as input. The developed models provide satisfactory predictions of both integral wave parameters and energy density spectra of sea and swell waves at the Chesapeake Bay entrance. The developed models can rapidly hindcast the wave characteristics and spectra during an extreme event (i.e., the Halloween storm in 1991). This paper provides a novel framework for developing surrogate models to predict wave spectra in the frequency domain and hindcast historical wave climate, which can be applied to other sea-crossing bridges and/or tunnel sites near bay entrances. The data-driven models, based on deep neural networks, allow for estimating waves without a high demand for computational resources, and thus serve as a useful tool for the characterization and simulation of the complex wave environment at the interface of estuary and ocean.

1. Introduction

Chesapeake Bay is the largest tidal estuary in the United States and the third-largest estuary in the world. The bay is approximately 320 km long between the northern headwaters in Havre de Grace, Maryland and the southern end in Norfolk, Virginia (Basco, 2020). The bay mouth is about 27 km wide from the City of Virginia Beach, Virginia, to the Eastern Shore of Virginia. The vehicle ferry services, which operated between the 1930s and early 1960s, carried travelers between the Norfolk/Virginia Beach area and Virginia's Eastern Shore. However, the ferries were time-consuming and impractical for the long-term needs of the region on the East Coast of the United States. Thus, the Chesapeake Bay Bridge-Tunnel (CBBT) was designed and constructed in the early 1960s. It first opened on April 15, 1964, which connects Virginia with Delaware and reduces 153 km of travel distance between these two states. The bridges sit above the water surface, and the tunnels are at the main shipping channels so that large vessels can efficiently go through the Chesapeake Bay entrance.

After more than half a century, The CBBT has become insufficient for the growing demand these days. As of 2020, the CBBT system consists of two tunnels, four artificial islands, and four bridges with lengthy causeways at both approaches (Designing buildings, 2020). Later expansions are planned to increase the tunnels and bridges' capacity (Designing buildings, 2020). To determine the design wave conditions for the maintenance and expansion of CBBT subject to the impact of global climate change, statistical analyses of long-term wave climate need to be performed. Although a program was launched to collect meteorological, oceanographic, and water-quality data through deploying buoys in Chesapeake Bay by the U.S. National Oceanic and Atmospheric Administration (NOAA) in 2007, there is still a lack of reliable long-term observations of surface waves in the Bay (Ti et al., 2022). Moreover, the wave system at the entrance of Chesapeake Bay is very complex because waves generated in the estuary and the Atlantic Ocean co-exist and transform over complex topography and strong tidal currents. Therefore, accurate modeling of future and historical wave characteristics is desirable.

E-mail address: q.chen@northeastern.edu (Q. Chen).

^{*} Corresponding author.

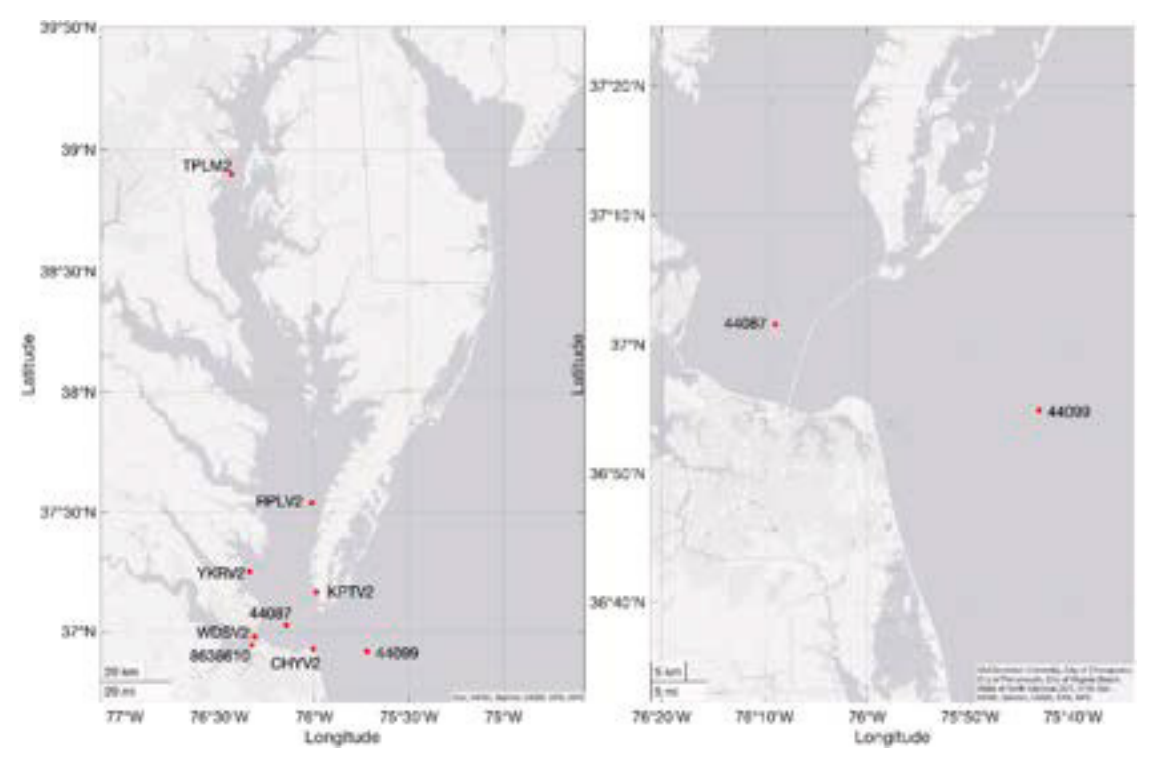


Fig. 1. (a) A map showing the Chesapeake Bay and locations of NDBC stations involved in this study. (b) A map showing the bay entrance and the locations of the NDBC stations 44,099 and 44,087 relative to the CBBT (marked as gray lines).

Wave characteristics are required in many engineering applications, such as designing sea-crossing bridges and tunnels, offshore wind farms, and pipelines, for the response, load, and fatigue calculations (Christakos et al., 2022). Normally, integral wave parameters, such as significant wave height, peak wave period, and mean wave direction, are used to characterize the sea state. Although the integral wave parameters are useful for describing trends in a series of observations, these quantities can smear the essential attributes of a wave field. They can be misleading when the wave conditions are complex with different wave systems propagating through a given area (Hanson and Phillips, 2001). On the other hand, wave energy density spectra can provide a more comprehensive way to describe the wave field, reveal more accurate information about waves from different origins, and help us better understand the surface wave conditions in coastal and estuarine areas.

In-situ measurement is often used to obtain wave spectra. However, field measurements are usually time-consuming to collect and spatially and temporally sparse because of high costs (e.g., Wang et al., 2022b; Ti et al., 2022). Therefore, physics-based wave models, such as SWAN (Booij et al., 1999), MIKE21 SW (DHI, 2017), and WAVEWATCH (Tolman and others, 2009), have been employed to simulate spatial and temporal evolutions of wave spectra in the ocean, coastal, and estuarine waters. Although numerical models can generate satisfactory estimations of waves in general, the direct application of these models to estimate wave spectra can have some drawbacks. For example, the simulation of localized wave and flow fields may require nested computational domains and/or coupled ocean circulation model and wave model, which can be extremely computationally expensive and not practical for a long-term assessment (e.g., yearly to multi-decadal). Additionally, some numerical approximations in these physics-based models, such as the approximate solutions to the quadruplet wave-wave interactions and triad interactions, may introduce errors in the model results (Song and Jiang, 2022). Alternatively, data-driven models can be used as surrogates to simulate wave spectra without a high demand for computational resources, and they can handle strong nonlinearity and high dimensionality (Wang et al., 2022a).

During the last two decades, many data-driven models have been developed to study nonlinear relationships between input features and labels for coastal and ocean engineering applications, such as artificial neural networks (ANN), decision trees, Bayesian networks, support vector machines, and long short-term memory (LSTM) (e.g., Deo and Naidu, 1998; Yagci and Kitsikoudis, 2015; Cornejo-Bueno et al., 2016; Sadeghifar et al., 2017; Oh and Suh, 2018; James et al., 2018; Stringari et al., 2019; Zheng et al., 2020; Callens et al., 2020; Mohaghegh et al., 2021; Tang and Adcock, 2021; Wei, 2021; Lee et al., 2021; Miky et al., 2021; Jo"rges et al., 2021; Elbisy and Elbisy, 2021; Bento et al., 2021; Huang et al., 2022; Bai et al., 2022; Wei and Davison, 2022). For instance, Zilong et al. (2022) proposed a novel data-driven model for efficient spatial-temporal significant wave height forecast in West Pacific using the LSTM method. Their model showed promising accuracy for wave height forecast and had higher computational efficiency than physics-based numerical models. Sakhare and Deo (2009) and Namekar and Deo (2006) applied support vector regression (SVR), model tree (MT), and ANN to obtain the wave spectra using significant wave height and wave period as input. Their results indicated that data-driven models could estimate the wave spectral shapes better than commonly used theoretical spectra, including Pierson-Moskowitz, JONSWAP, and Scotts. Song and Jiang (2022) established a deep neural network to estimate directional wave spectra using local and remote wind fields as input. They found that the model can predict the local wave spectra with low computational cost and perform well in predicting spectral shape. These data-driven models provide a new method to solve wave prediction problems in coastal and estuarine areas.

This paper is dedicated to estimating integral wave parameters and energy density spectra near the CBBT at the Chesapeake Bay entrance using advanced scientific machine learning (ML) techniques. Specifically, we focus on predicting the desired wave properties at the National Data Buoy Center (NDBC) station 44,087, 5 km west of the CBBT. Unlike previous works which used integral wave parameters or winds as input features (i.e., Sakhare and Deo (2009), Namekar and Deo (2006), and Song and Jiang (2022)), wind, water level, and offshore wave data

Table 1
Wind, water level, and wave buoy stations involved in this study.

Туре	Station name
Wind station (NDBC)	TPLM2, RPLV2, YKRV2, KPTV2, WDSV2, and CHYV2
Water level station (NOAA)	8638,610 at Sewells Point, VA
Wave buoy station (NDBC)	44,087 and 44,099

were used as input features for developing novel composite ANN models for wave spectral predictions in this study. To resolve the complex wave field at the bay entrance, we separated the wave fields at the two NDBC stations into bay waves (generated in the bay) and ocean waves (coming from the ocean) based on the two-dimensional (2D) wave spectra in the frequency and directional spaces. The developed models were then applied to hindcast the wave characteristics and spectra at the study site during the Halloween storm in 1991. The models allow for estimating waves without a high demand for computational resources. This paper presents a novel framework as a surrogate to estimate wave spectra in the frequency domain and hindcast historical waves. This framework can be applied to other sea-crossing sites near a bay entrance.

The rest of the paper is organized as follows. Section 2 presents the model development, including model input, output, and model setup. Section 3 examines the performance of the ML models in estimating integral wave parameters and energy density spectra for both bay and ocean waves by comparing the model outputs with the field measurements. The wave hindcast at the study site during the Halloween storm, or the so-called "perfect storm" in 1991, is also presented in this section. The influence of wind fields and offshore waves on the accuracy of hindcasted waves during the Halloween storm is discussed in Section 4. A representativeness test of the training data is also conducted to ensure the predicted wave spectra and characteristics during the Halloween storm are reasonable. Finally, Section 5 concludes the paper with remarks on this study.

2. Methods

2.1. Study area

The study site is near the mouth of Chesapeake Bay (Fig. 1). The NDBC buoy station 44,087 is located roughly 5 km west of the CBBT, and thus the wave field at buoy 44,087 is pragmatically used to represent the wave field around the CBBT. The NDBC buoy station 44,099, located approximately 26 km southeast of the bay entrance (Fig. 1(b)), provides representative offshore wave fields out of the bay. As there is a lack of reliable long-term (multi-decadal) wave observations in Chesapeake Bay (Ti et al., 2022), an accurate forecast of upcoming or hindcast of historical wave conditions at buoy 44,087 can be very useful for structural design and assessment purposes. Four artificial islands connecting the bridges and tunnels were built with 10-ton armor stones, which are relatively stable and have survived many tropical cyclones since 1964 (Basco, 2020). However, severe damage to the revetment was observed at one location on the south CBBT island on October 31, 1991, during the Halloween storm, a severe Nor'easter storm.

2.2. Wind, water level, and wave measurements

This study used the wind, water level, and offshore wave measurements as input features to develop ML models for estimating wave parameters and spectra near the entrance of Chesapeake Bay (Fig. 1, Table 1). The water level data were obtained from NOAA 8638,610 at Sewells Point, VA. It is well known that the growth of waves in an estuary is influenced by water depth (i.e., wave height is limited in the finite depth condition). The wind data were achieved from six NDBC stations scattered over the bay (i.e., TPLM2, RPLV2, YKRV2, KPTV2, WDSV2, and CHYV2), and more details can be found in Section 2.2.1. The 2D wave spectra data at the buoys 44,099 and 44,087 were obtained

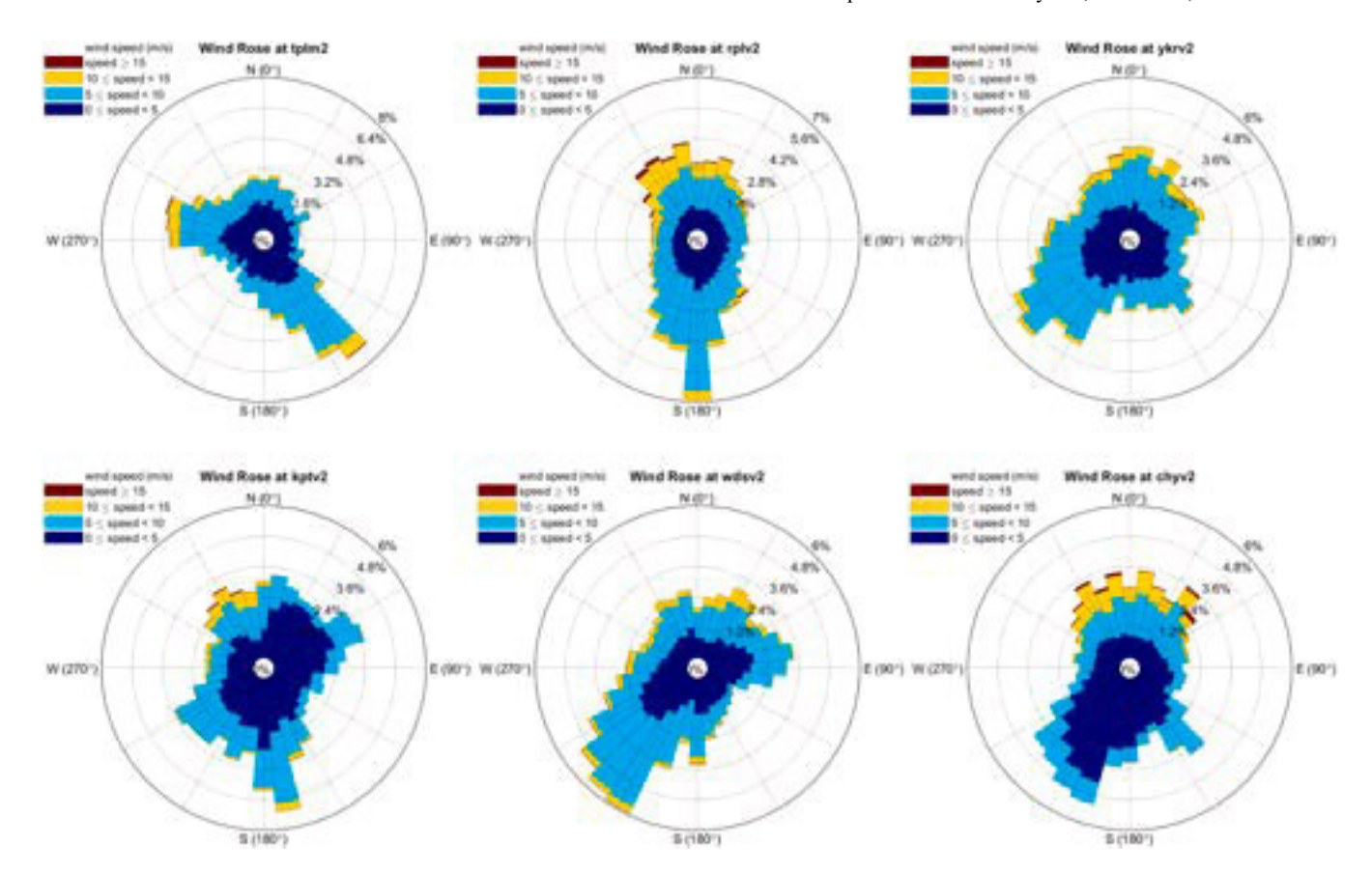


Fig. 2. Wind roses at NDBC Stations TPLM2, RPLV2, YKRV2, KPTV2, WDSV2, and CHYV2 based on measurements from 2020 to 2021.

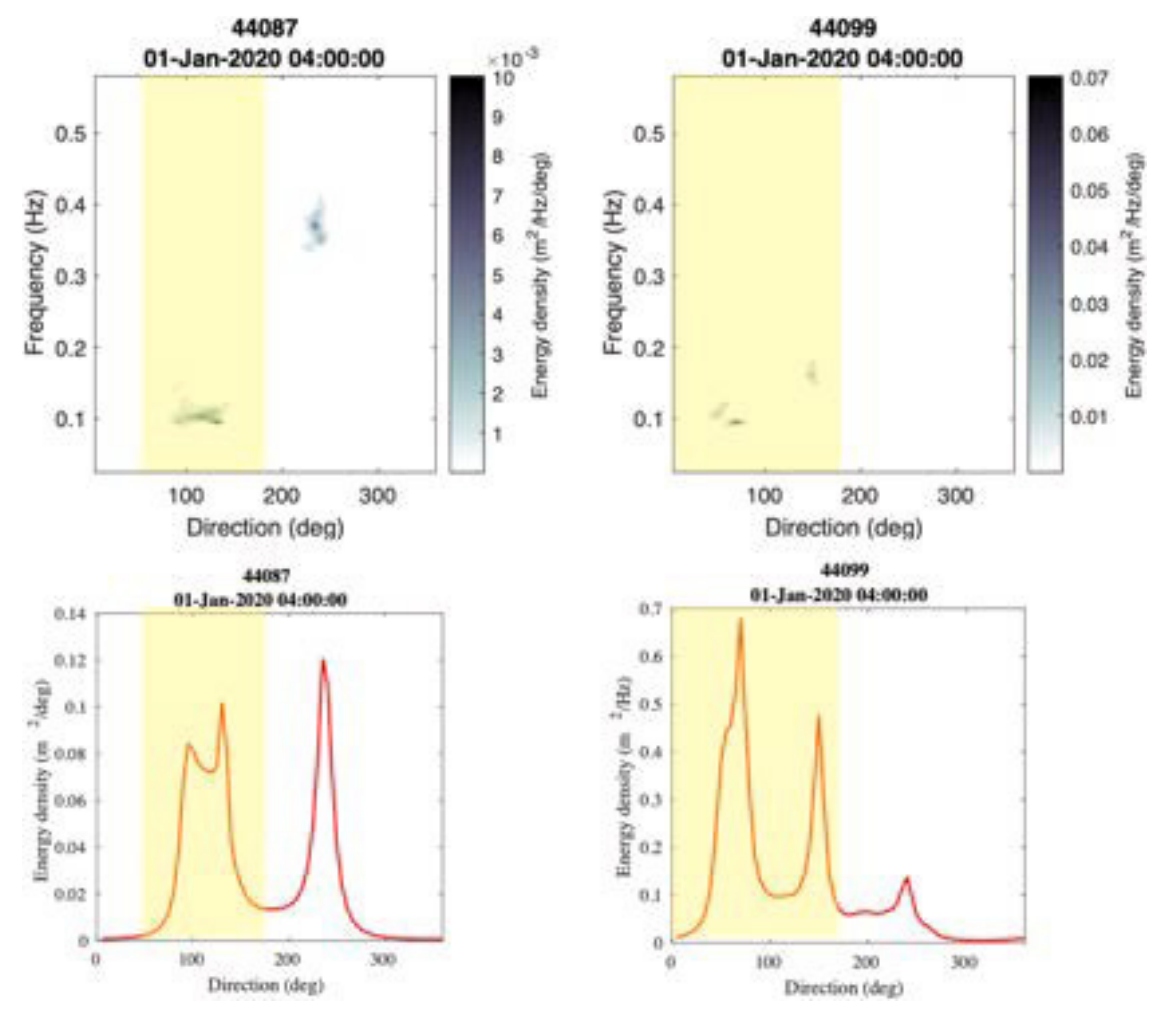


Fig. 3. Example of separating bay and ocean energy from the 2D wave spectra at the buoys 44,087 and 44,099. The shaded areas represent the energy of ocean waves. The rest of the energy is associated with bay waves.

from the Coastal Data Information Program (CDIP). The buoys 44,099 and 44,087 were deployed on 07/23/2008 and 08/06/2018, respectively. Wave data at buoy 44,087 are unavailable prior to its deployment (i.e., 08/06/2018). The developed composite ANN models can help estimate a longer history of wave characteristics at buoy 44,087. Also, this model can provide a hindcast of wave characteristics during the Halloween storm in 1991, which facilitates the assessment of wave impact on the CBBT during extreme events.

2.2.1. Spatial variation of winds in Chesapeake Bay

Wind is the main driving force of surface waves. To account for the large variability of wind speed and direction in the bay area (Mariotti et al., 2018), wind measurements from six NDBC stations scattered over the bay (i.e., TPLM2, RPLV2, YKRV2, KPTV2, WDSV2, and CHYV2 in Fig. 1(a)) were collected. These stations were selected considering their locations and data availability. The wind roses based on the measurements at these six stations indicate tremendous spatial variations of wind fields inside Chesapeake Bay (Fig. 2). More details of model inputs regarding wind data can be found in Sections 2.3.1 and 2.3.2.

2.2.2. Partition of bay and ocean waves

In this study, the waves at NDBC Stations 44,099 (denoted as the offshore buoy) and 44,087 (denoted as the bay buoy) were partitioned into bay and ocean waves based on the 2D wave spectra in the frequency and directional spaces. Considering the locations of both buoys and the shoreline of the Chesapeake Bay entrance (Fig. 1(b)), the wave energy

coming from 50°-180° and 0°-180° (0° is the true north) was set as ocean waves (coming from the ocean) for the bay buoy 44,087 and offshore buoy 44,099, respectively. The rest of the energy was identified as bay waves (generated in the bay). Fig. 3 presents an example showing how to separate the 2D spectra into bay and ocean waves at both buoys.

2.3. Data-driven models

To determine the wave characteristics and energy density spectra at bay buoy 44,087, we developed two data-driven models based on deep neural networks for predicting bay and ocean waves separately using wind, water level, and offshore waves at offshore buoy 44,099 as input features. Then the developed ANN models were used to estimate waves at the bay buoy during the Halloween storm in 1991, when the recorded waves were unavailable. Based on Karimpour et al. (2017), there is a strong relation between wave height, water depth, and wave period. All three parameters are related. Therefore, composite models were developed with the total loss function defined as the sum of the error functions of each target (i.e., H_{m0} , T_p , Dir, and E). Although independent networks could also be utilized to predict H_{m0} , T_p , Dir, and E separately, they were not used in this work because of the error propagation from one network to another (Wang et al., 2022). Table 2 lists the input features and labels for estimating bay and ocean waves at bay buoy 44, 087. Fig. 4 sketches the architecture of the composite neural networks. For the bay wave prediction, the measured hourly u- and v-wind speed components and water level were used as input features to esti-

Input features and labels for predicting integral wave parameters and spectral

energy in the frequency domain for bay and ocean waves at buoy 44,087. $H_{m0, in}$, $T_{p, in}$, Dir_{in} , and E_{in} represent the wave parameters and spectra values at NDBC station 44,087. $H_{m0, out}$ and $T_{p, out}$ represent the wave parameters at NDBC station 44.099.

	Prediction	Input features	Labels
Bay waves	$H_{ m m0,\ in}$	u- and v-wind speed data at TPLM2, RPLV2, YKRV2, KPTV2, WDSV2, and CHYV2, water level data at Sewells Point	Measured $H_{ m m0,in}$
	T _{p, in}	u- and v -wind speed data at TPLM2, RPLV2, YKRV2, KPTV2, WDSV2, and CHYV2, water level data at Sewells Point, predicted $H_{\rm m0,in}$	Measured $T_{p,in}$
	Dir in	u- and v -wind speed data at TPLM2, RPLV2, YKRV2, KPTV2, WDSV2, and CHYV2, water level data at Sewells Point, predicted $H_{m0,in}$	Measured $\sin(Dir_{in})$ and $\cos(Dir_{in})$
	E in	u - and v -wind speed data at TPLM2, RPLV2, YKRV2, KPTV2, WDSV2, and CHYV2, water level data at Sewells Point, predicted $H_{\rm m0,in}$ and $T_{\rm p,in}$	Measured E_{in}
Ocean waves	$H_{ m m0,\ in}$	u - and v -wind speed data at KPTV2 and CHYV2, water level data at Sewells Point, measured $H_{\rm m0,out}$ and $T_{\rm p,~out}$	Measured $H_{ m m0,in}$
	$T_{ m p,\ in}$	u - and v -wind speed data at KPTV2 and CHYV2, water level data at Sewells Point, measured $H_{\rm m0,out}$ and $T_{\rm p,\ out}$, predicted $H_{\rm m0,in}$	Measured $T_{p,in}$
	E in	u- and v -wind speed data at KPTV2 and CHYV2, water level data at Sewells Point, measured $H_{\rm m0,out}$ and $T_{\rm p,\ out}$, predicted $H_{\rm m0,in}$	Measured E_{in}

mate the zero-moment wave height H_{m0} . As H_{m0} interrelates with the peak wave period T_p and mean wave direction Dir, H_{m0} was further used as an input together with the wind and water level for simulating T_p and Dir. The spectral wave energy values in the frequency domain (E) were

determined with the wind, water level, H_{m_0} , and T_p applied as the input features. The total loss function for predicting bay waves was defined as the sum of error functions of H_{m0} , T_p , Dir, and E. Note that $\sin(Dir)$ and cos(Dir) were employed to represent the wave direction Dir in the neural networks ($Dir = 0^{\circ}$ and 360° are the same). For ocean wave estimation at bay buoy 44,087, we included $H_{\rm m0}$ and $T_{\rm p}$ of ocean waves measured at the offshore buoy 44,099 as input, since ocean waves measured at buoys 44,099 and 44,087 were correlated. The prediction of ocean wave directions was not included in this study, because the ocean wave directions are within a narrow range due to the wave refraction and shoreline sheltering effects (Section 2.3.2). Thus, the corresponding loss function for estimating ocean waves at the bay buoy location was determined as the sum of error functions of H_{m0} , T_p , and E. The definitions of H_{m0} , T_p , Dir, and E can be found in Table A1 in Appendix.

The 2D wave spectra in frequency and direction spaces at NDBC buoys 44,099 and 44,087 were estimated from the first-five Fourier coefficients with spectral reconstruction methods (Earle et al., 1999). However, the reconstructed 2D spectra through these methods can be noisy at different frequency and direction bins (Song and Jiang, 2022). To develop an ANN model with better performance for estimating the spectral energy values for both bay and ocean waves, we smoothed the frequency spectra with a sliding window size of 6. The sensitivity of the integral parameters to the smoothed frequency spectra was examined. The results show that the integral wave parameters H_{m0} and T_p derived from the original and smoothed spectra are very close (Fig. A1). Thus, the smoothed frequency spectra at buoys 44,087 and 44,099 were employed to develop composite ANN models for predicting integral wave parameters and spectra of bay and ocean waves at bay buoy 44,

Because the network structure can largely influence the prediction performance of ANNs, a total of 1164 structures (2-5 hidden layers with 10-300 nodes per layer) were examined to identify the optimal network structures for simulating integral parameters and spectra of bay and ocean waves (Wang et al., 2022c). The number of hidden layers and nodes for networks to simulate H_{m0} , T_p , Dir, and E was kept the same. The total composite performance score (TCPS) was evaluated based on error matrices, including bias, SI, and R², so that the prediction performance of different structures can be quantified (Table A2).

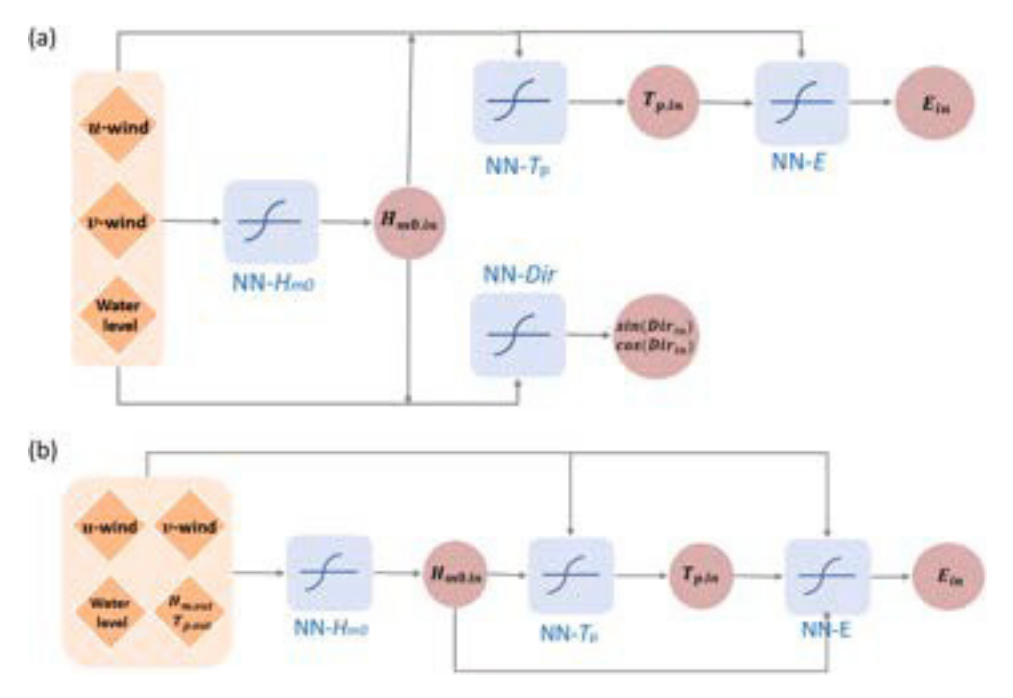


Fig. 4. Schematic architecture of the composite neural networks for predicting H_{m0} , Tp, Dir, and E of (a) bay waves and (b) ocean waves at buoy 44,087. $H_{m0,in}$, $T_{p,ib}$ Dir in, and E in represent the wave parameters and spectral energy at NDBC station 44,087. Hm0,out and Tp, out represent the wave parameters at NDBC station 44,099.

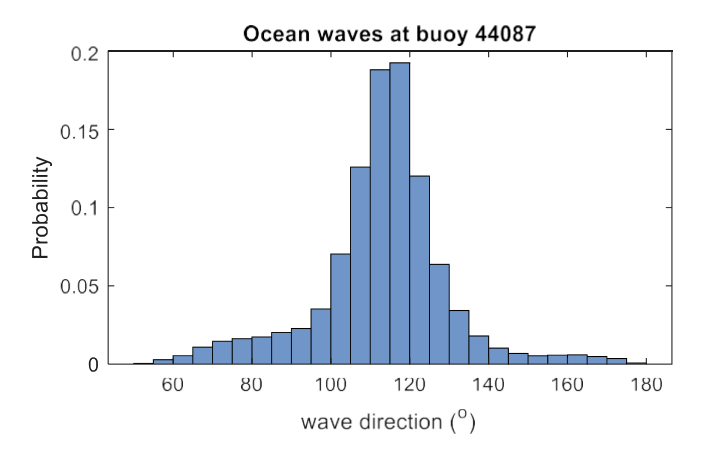


Fig. 5. The probability density plot for measured ocean wave directions at buoy 44,087 from 2018 to 2021.

2.3.1. Prediction of bay waves

In this study, a composite wave model was trained and validated to estimate $H_{\rm m0}$, $T_{\rm p}$, Dir, and E of bay waves based on the measured integral wave parameters and spectra at bay buoy 44,087 from August 2018 to December 2021. The testing and validation data contained continuous hourly datasets from 09/01/2021 to 11/01/2021 and 06/01/2021 to 08/01/2021, respectively. The training data were the rest of the dataset from 2018 to 2021. Because bay waves are essentially locally generated wind waves in Chesapeake Bay, small, swell-like waves with $H_{\rm m0} < 20$ cm and $T_{\rm p} > 6$ s were excluded from the training data.

Pytorch (https://pytorch.org/) was applied to develop the composite network to estimate bay waves in this study. Hyperbolic Tangent was used as the activation function. The mean square error (MSE) of predicted parameters and maximum learning epoch were employed to control the training procedure. Specifically, the training procedure was stopped once the iteration number reached 2000 or one of the MSEs of H_{m_0} , T_p , Dir, and E stopped to decrease. To avoid the negative effect of the large difference between various parameters, we applied normalization to keep inputs and outputs between -1 and 1. The initial biases in each layer were all set to zero, and the initial weights were set to follow Xavier normal distribution (Glorot and Bengio, 2010). The initial learning rate was 0.01 and then decreased to 0.001 after 500 iterations. The training was conducted on an Intel Core i9 CPU with 32 GB memory, and the training time was approximately 60 s.

2.3.2. Prediction of ocean waves

Compared to the ANN model setup for estimating bay waves, the main difference of the deep neural network for ocean waves is that wave direction is not one of the outputs. This is because ocean wave directions are within a narrow range (100° to 130°) due to the wave refraction and shoreline sheltering effects. Fig. 5 shows that about 76% of ocean waves came from a direction within the range of 100-130 °. Additionally, only the wind data from the nearby two stations (i.e., KPTV2 and CHYV2) were included in the input features, because the other stations may not well represent the wind coming from the ocean to the study site. Moreover, the waves measured at the offshore buoy 44,099 outside the bay have close correlations with the ocean wave components measured at the bay buoy 44,087. Therefore, the wave parameters, including H_{m0} and T_p at the offshore buoy 44,099, were applied as input features as well. The testing, validation, training data, and other model setups for developing the ANN model for ocean waves were kept the same as the ones used in the ANN model for bay waves.

2.3.3. Hindcasting waves during the Halloween storm in 1991

The Halloween storm was a devasting Nor'easter that initially developed off the coast of Atlantic Canada on October 28 and fully dissipated late on November 2, 1991. In this study, the validated models

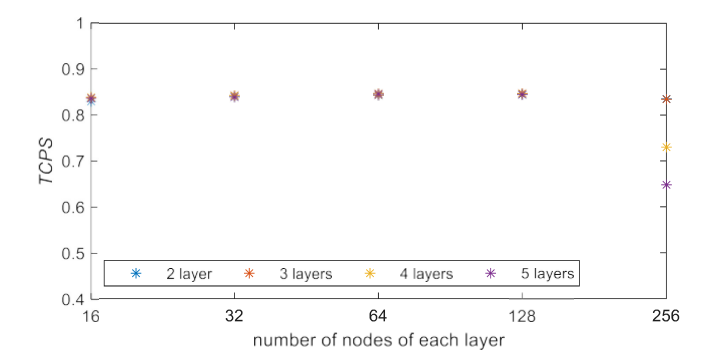


Fig. 6. The TCPSs generated by the composite wave models for bay wave predictions using different network structures.

were applied to hindcast waves during this storm. As mentioned in Section 2.3, the wind data measured at six NDBC stations were employed to develop the composite ANN model to predict bay waves at the study site. As the NDBC wind data in 1991 are unavailable, we collected the wind data from the National Centers for Environmental Prediction (NCEP) Climate Forecast System Reanalysis (CFSR) (Saha et al., 2010b, 2014). The CFSR was designed and executed as a global, high-resolution, coupled atmosphere-ocean-land surface-sea ice system, providing estimates of the state of coupled domains from 1979 to 2009. The spatial resolution of CFSR is approximately 38 km, and the CFSR atmospheric, oceanic, and land surface output products are available hourly. Therefore, we selected the nearest grids to the NDBC stations for extracting the wind data in 1991 from the CFSR datasets (Saha et al., 2010a). The water level data in 1991 are available at NOAA station 8638,610.

The offshore wave data at station 44,099 in 1991 is required to hindcast ocean waves during the Halloween storm. As the measured wave data at station 44,099 are unavailable in 1991, we used the dataset of WAVEWATCH III® 30-year Hindcast Phase 2 (WWIII), which also applies the NECP CFSR wind as model input and covers the time period from 1979 through 2009. The output from the WWIII buoy files contains the hindcasted wave spectra at the offshore buoy 44,099. The WWIII spectra have different resolutions of frequency and direction domains compared to the measured wave spectra at buoy 44,099. Thus, the WWIII spectra were firstly interpolated to obtain the same resolutions in frequency and direction spaces as those measured. Then, the developed model was applied to hindcast ocean waves at bay buoy 44,087 based on the CFSR wind data and WWIII wave data in 1991 and beyond.

3. Results

3.1. Integral wave parameter predictions of bay and ocean waves

A total of 1164 structures (2–5 hidden layers with 10–300 nodes per layer) were examined to identify the optimal network structures for simulating integral parameters and spectra. Fig. 6 shows an example of *TCPS*s generated by selected composite wave models using various network structures (2–5 hidden layers with 8, 16, 32, 64, 128, and 256 nodes per layer) for bay wave predictions. It can be observed that the model skills are similar when the networks have 2 or 3 hidden layers (Fig. 6). Overfitting patterns can be observed when the structure has 3 or 4 layers with more than 160 nodes per layer. The optimal structures for simulating bay and ocean waves were determined as 3 layers of 20 nodes and 3 layers of 36 nodes, respectively (the highest TCPSs for bay and ocean waves are 0.85 and 0.79, respectively).

The comparisons between the simulated and measured $H_{\rm m0}$, $T_{\rm p}$, and Dir during the testing phase are shown in Fig. 7(a). The composite wave model shows a high prediction skill for estimating $H_{\rm m0}$ of bay waves at the bay buoy 44,087, with an R² value of about 0.87 and a root mean square error (RMSE) of about 0.08 m. The simulation accuracy of $T_{\rm p}$ of

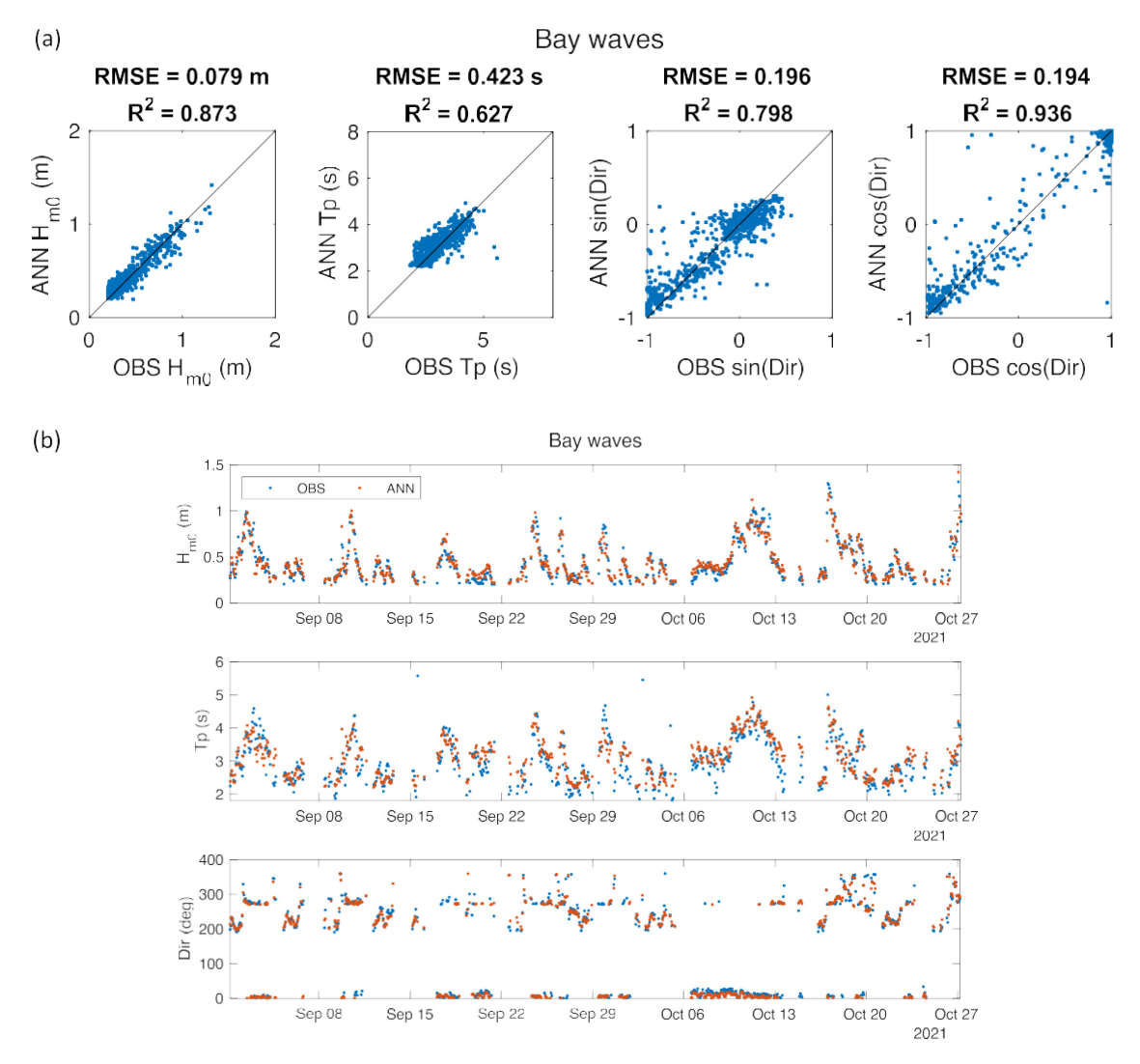


Fig. 7. Comparison between the measured and simulated H_{m0} , T_p , and Dir of bay waves at the bay buoy 44,087. (a) Scatter plots and (b) time series (only contain the testing data). $\sin(Dir)$ and $\cos(Dir)$ were employed to represent the wave direction Dir in the neural networks ($Dir=0^{\circ}$ and 360° are the same). The third panel in (b) shows the comparison between the measured and simulated Dir converted from $\sin(Dir)$ and $\cos(Dir)$.

bay waves is slightly lower, with R^2 values around 0.63 and RMSE around 0.42 s. Notice that most of the existing data-driven wave models were only focused on significant wave height prediction because of the difficulty in predicting peak wave periods. Our proposed composite model also shows a good performance in predicting the bay wave direction. For ocean wave prediction, the composite deep neural networks produce satisfactory results for simulating both $H_{\rm m0}$ and $T_{\rm p}$ at the bay buoy 44,087 (Fig. 8(a)), with R^2 values around 0.90 and 0.72, respectively. The time series of the predicted and observed wave parameters of the bay and ocean waves during the testing phase are presented in Figs. 7 (b) and 8(b). Good agreement between the modeled and measured $H_{\rm m0}$, $T_{\rm p}$, and bay wave Dir is achieved. Thus, the composite ANN models can be used to forecast or hindcast integral wave parameters with sufficient accuracy for both bay and ocean waves at the study site.

3.2. Predictions of energy density spectra of bay and ocean waves

The composite networks also provide estimations of wave spectra in frequency space. Fig. 9 presents the comparisons between the simulated and measured spectral energy density values of bay and ocean waves at buoy 44,087. The model results show good agreement with the field measurements, with RSEM around 0.034 and 0.029 m²/Hz for bay and ocean waves, respectively. Fig. 10 depicts six examples of the estimated

and measured wave spectra of bay and ocean waves. It is seen that the composite models can capture the shapes of wave spectra. To further investigate the model performance, two additional parameters were calculated to determine the differences between the observed and predicted wave spectra, including the peak energy density ($E_{\rm max}$) and spectral width ($S_{\rm width}$). $E_{\rm max}$ is defined as the maximum spectral energy density in the frequency domain (Dabbi et al., 2015). $S_{\rm width}$ represents the narrowness of a wave energy density spectrum (if this parameter is closer to one, the spectrum is narrower) (Rogers and Van Vledder, 2013). More details of the definitions of these two parameters can be found in Table A1. Fig. 11 shows the time series of the simulated and measured $E_{\rm max}$, $S_{\rm width}$, and the corresponding $H_{\rm m0}$. Overall, the good model-data agreement further demonstrates the composite models are capable of predicting wave spectra of both bay and ocean waves with high accuracy.

3.3. Hindcast of wave spectra during the Halloween storm (1991)

This section demonstrates an application of the composite models to assess the damages from the Halloween storm (1991) to the CBBT. We estimated the wave spectra of both bay and ocean waves at bay buoy 44,087 during the storm using the developed composite ANN models. Time series of the estimated $H_{\rm m0}$ and $T_{\rm p}$ of bay and ocean waves are

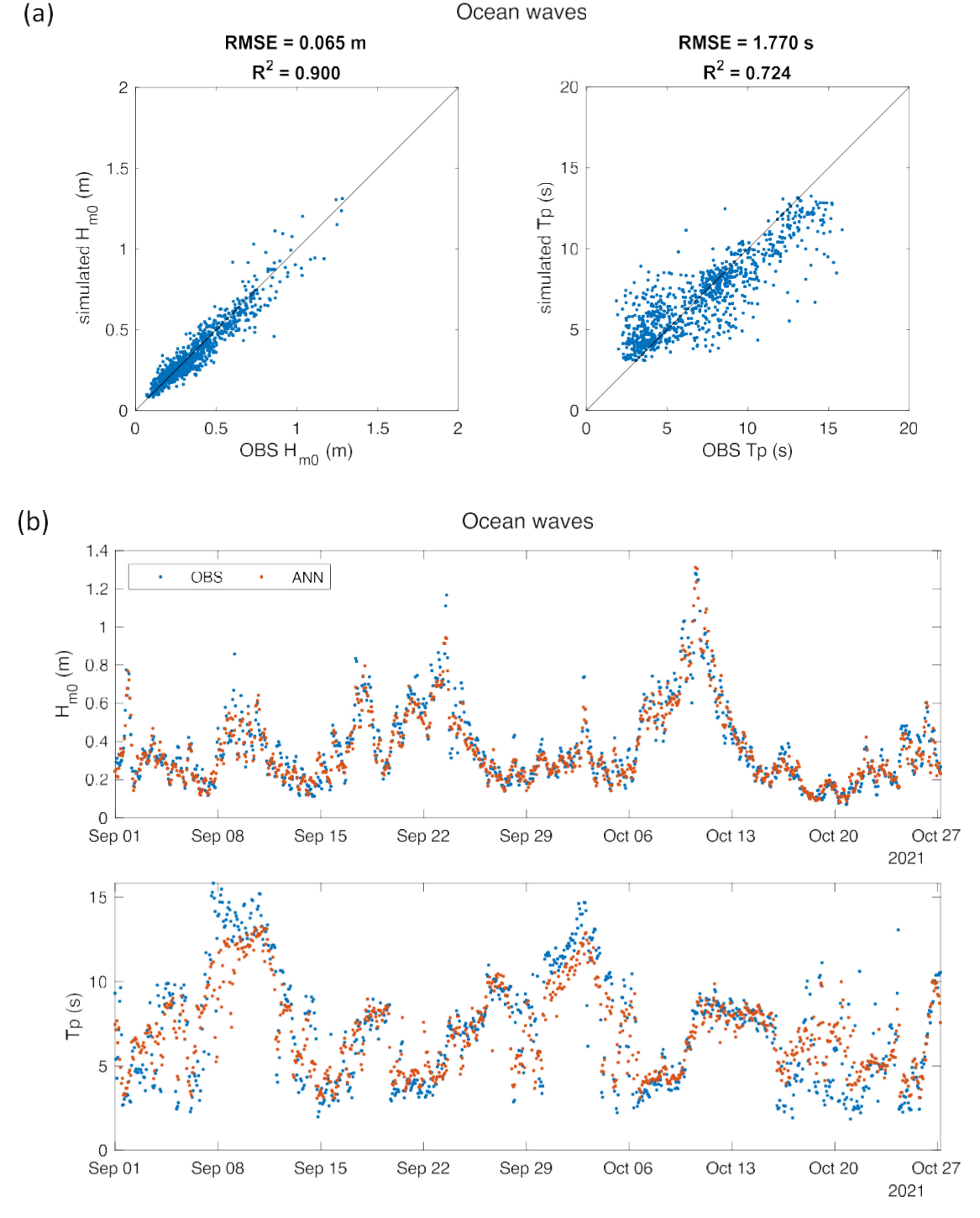


Fig. 8. Comparison between the measured and simulated H_{m0} and T_p of ocean waves at the bay buoy 44,087 (a) Scatter plots and (b) time series (only contain the testing data).

shown in Fig. 12. The model results indicate that the maximum $H_{\rm m0}$ of ocean waves was about 1.4 m during the storm, which was about twice larger than that of the bay waves (occurred on October 29, 1991, 03:00). We also found that $T_{\rm p}$ and $H_{\rm m0}$ of ocean waves did not reach their peak values simultaneously, and the predicted ocean wave $T_{\rm p}$ reached its peak value at 06:00 on October 31, 1991. Three examples of the hindcasted wave spectra of bay and ocean waves are shown in Fig. 13. It can be observed that the energy of ocean waves was much higher than that of bay waves, indicating that the devastating wave energy near the CBBT mostly came from the Atlantic Ocean during the storm. This finding is consistent with the fact that the Nor'easter wind blowing from the

northeast does not generate large bay waves considering the geometry and dimension of Chesapeake Bay.

4. Discussion

4.1. Representativeness test for training data

One of the drawbacks of ANN models is the inability to do extrapolation (cannot generalize to estimate scenarios that are unseen in the training dataset). Therefore, we examined whether the offshore waves at buoy 44,099 and wind conditions from August 2018 to December 2021

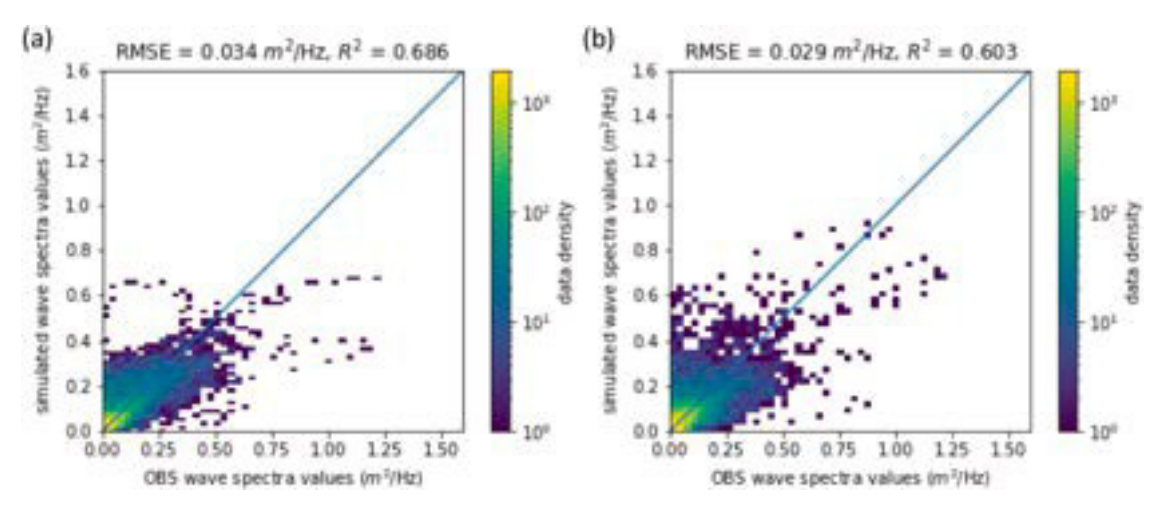


Fig. 9. The comparison between the observed and simulated wave spectra for (a) bay and (b) ocean waves at the buoy inside the bay (only contain the testing data).

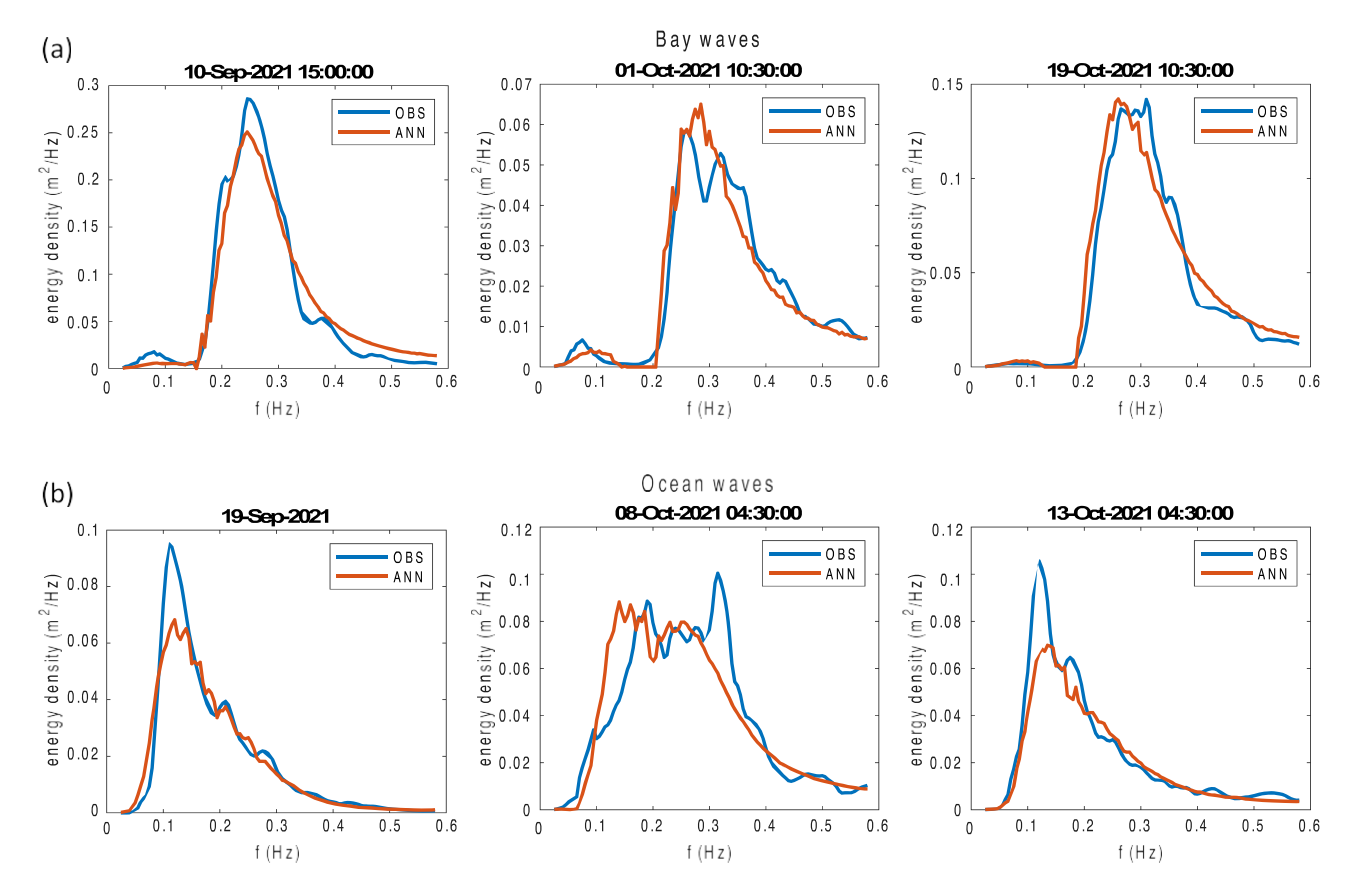


Fig. 10. Comparisons between the measured and simulated bay and ocean wave spectra at selected times during the testing phase at buoy 44,087.

(the data we used to develop ANN models) can represent the ones during the storms in October and November 1991. It was found that the largest measured $H_{\rm m0}$ at buoy 44,099 (4.64 m) during the training period is higher than the one from WWIII (2.8 m) during the Halloween storm in 1991, and there were about 0.7% of the training data with $H_{\rm m0}$ values larger than 2.8 m.

For the wind fields, we compared the wind conditions from August 2018 to December 2021 (41 months) and the ones from October to November 1991 (during the Halloween storm). The following steps were taken to quantify the representativeness of the forcing of wave generation during the storm (Wang et al., 2022c). Firstly, the hourly datasets of wind direction and wind speed during the two months in 1991 and from

August 2018 to December 2021 were uniformly divided into 36 directional bins at 10° intervals (i.e., $0^\circ-10^\circ$, ...,350°-360°) and 60 speed bins at 0.5 m/s intervals (i.e., $0^\circ-10^\circ$, ..., 29.5-30 m/s), respectively (Fig. 14). The two groups of bins were then combined into 2160 divisions (i.e., $36\times60=2160$). A wind forcing was considered representable by the 41-month forcings if that specific data fell into one of the divisions that were also taken by the 41-month data. The results show that during the two months in 1991, the average percentage of winds that could be represented by the data from 2018 to 2021 is about 97.6% at the six wind stations (Table 3). As the offshore waves and wind conditions in Chesapeake Bay from August 2018 to December 2021 could largely represent the ones during the Halloween storm, it can be

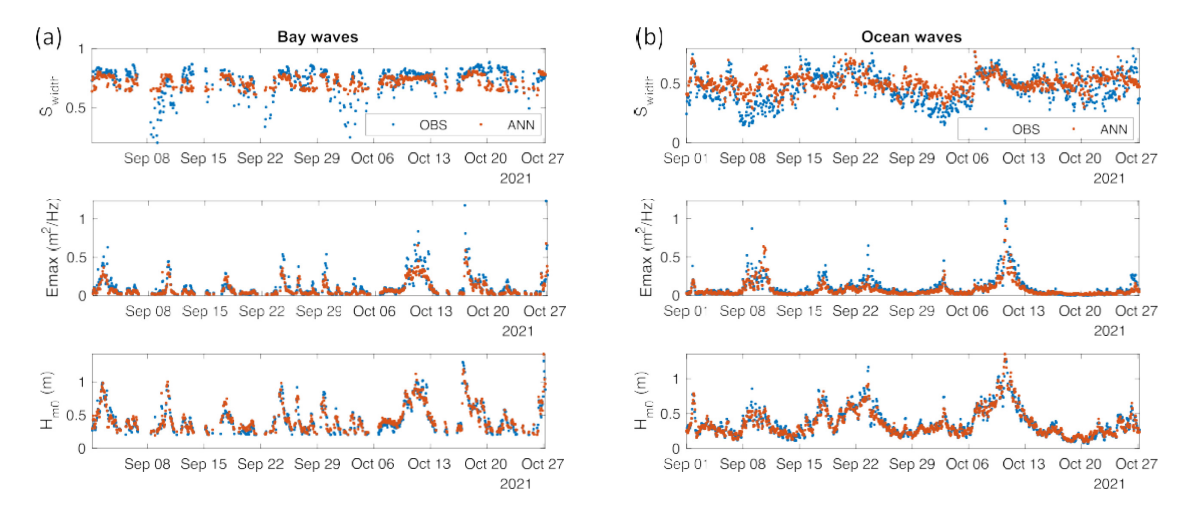


Fig. 11. Time series of simulated and measured Swidth, Emax, and Hm0 of (a) bay and (b) ocean waves at bay buoy 44,087.

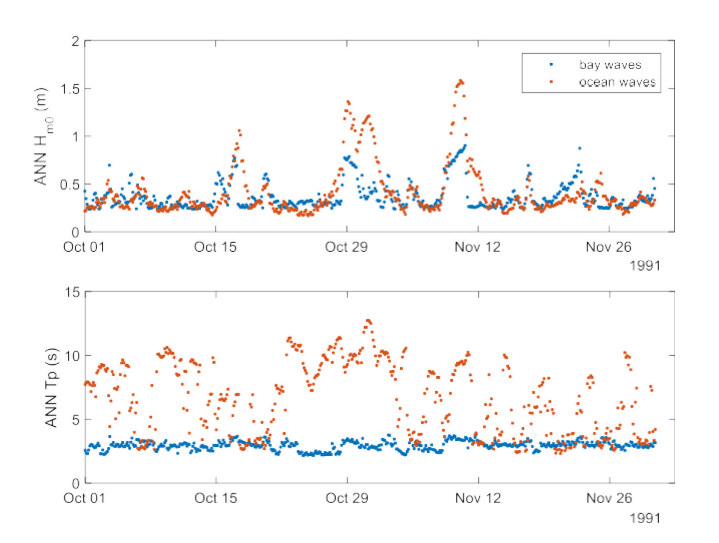


Fig. 12. The time series of ANN-predicted H_{m0} and Tp at bay buoy 44,087 in October and November 1991.

expected that the composite ANN models are capable of hindcasting wave parameters and spectra with sufficient accuracy at the bay buoy 44,087 during the 1991 storm if the input CFSR winds and WWIII waves were accurate.

4.2. Potential hindcast errors during the Halloween storm

In this study, the developed ANN models were utilized to estimate the integral wave parameters and energy density spectra at bay buoy 44,087 during the Halloween storm in 1991. According to Basco (2020), very long period swell waves were observed during the storm. For example, $H_{\rm m0}=2.6$ m and $T_{\rm p}=23$ s were measured at the Virginia Beach wave gage (VA001), and $H_{\rm m0}=4.6$ m and $T_{\rm p}=22$ s were reported at the U.S. Army Corps of Engineers, Field Research Facility (FRF) at Duck, North Carolina. However, the largest values of estimated $H_{\rm m0}$ and $T_{\rm p}$ of ocean waves hindcasted by the developed ANN models are 1.4 m and 12.7 s, respectively, which are lower than the estimates inferred from the CBBT armor unit damage in Basco (2020). The difference between the inferred wave height and the hindcast can be explained by the following reasons.

Firstly, the ANN models were developed with the wind data measured at the NDBC stations. Because the NDBC wind and wave data at the offshore buoy 44,099 were unavailable in 1991, the CFSR reanalysis wind data and the WWIII hindcast were utilized as input to hindcast the wave conditions during the storm. Although the wind data at the nearest grids to the NDBC stations were used as input to hindcast bay and ocean waves, the wind forcings extracted from CFSR may not well represent the real wind conditions at the locations of NDBC stations. This mainly affected the bay wave prediction. Secondly, the WWIII hindcasted wave spectra used as input for ocean wave predictions may also contain errors. For instance, the longest wave period output from WWIII is about 16.7 s during the storm, much shorter than the

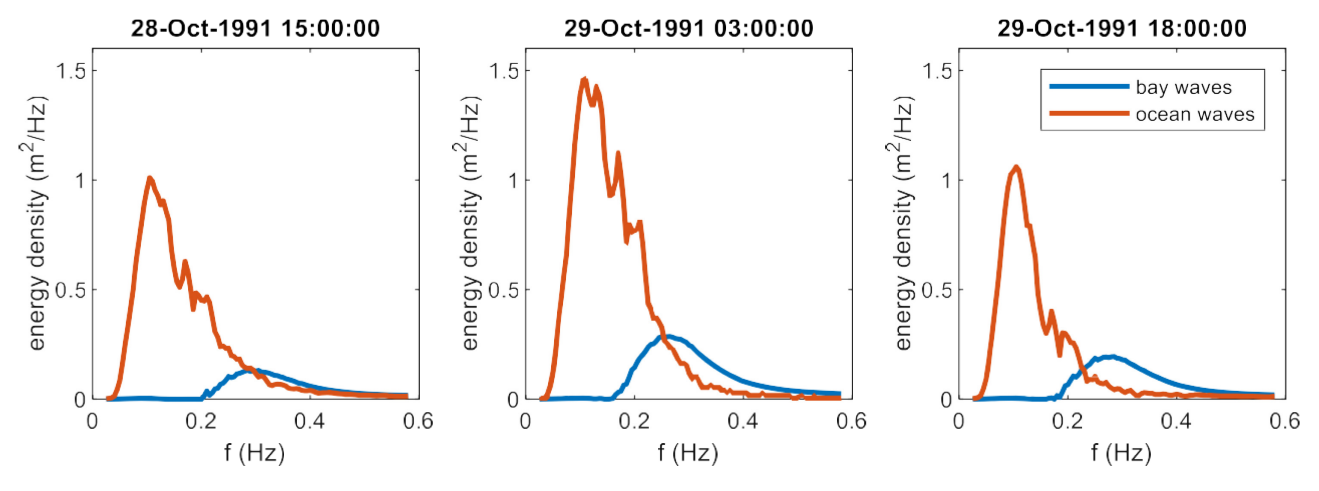


Fig. 13. Examples of the hindcasted bay and ocean wave spectra during the Halloween storm in 1991 using composite ANN models.

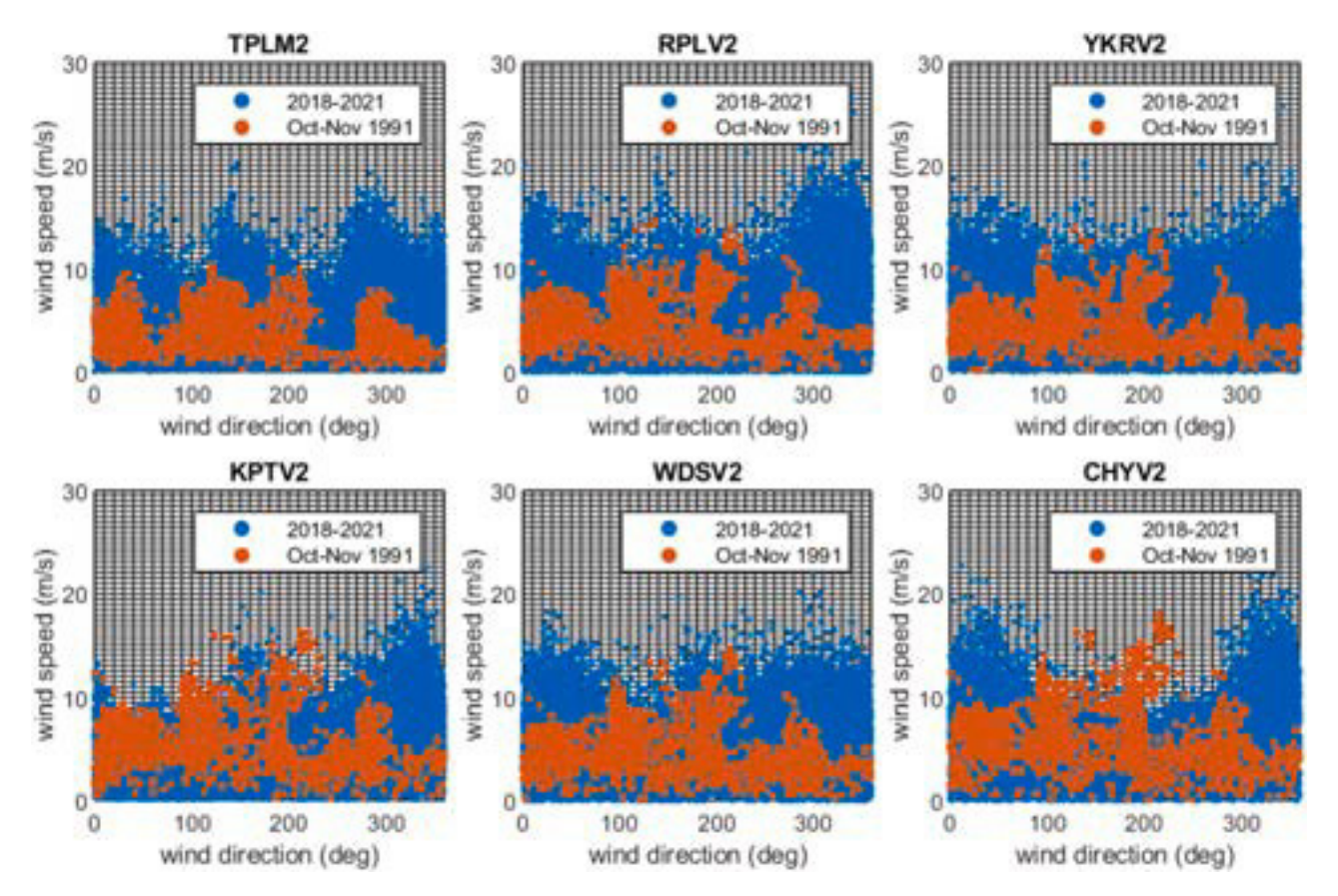


Fig. 14. Wind direction and wind speed at different stations in October and November 1991 versus August 2018 to December 2021.

Table 3Percentages of wind data at different CFSR grids in October and November 1991 that can be represented by the NDBC wind data from August 2018 to December 2021.

Station	TPLM2	RPLV2	YKRV2	KPTV2	WDSV2	CHYV2
Percentage	100.0%	99.7%	99.8%	95.6%	99.9%	90.9%

measurements at the VB gage VA001 and the FRF. Thus, the uncertainty in the CFSR and WWIII results can induce simulation errors in the hindcast of the bay and ocean waves at bay buoy 44,087 during the storm. Thirdly, the spatial variability of the wave field near the bay entrance and along the coast could be substantial due to the strong variations in bathymetry and currents. Notice that the study site at bay buoy 44,087 is about 5 km northwest of the CBBT (Fig. 1). The four artificial islands and bathymetric variation could also affect the wave field. Therefore, the real wave height at bay buoy 44,087 is likely different from the measurements at VB gage VA001 and the FRF during the storm.

5. Summary and conclusions

Chesapeake Bay is the largest tidal estuary in the United States, with the bay mouth width of about 27 km from the City of Virginia Beach to the Eastern Shore of Virginia. To reduce the travel distance between the states of Virginia and Delaware, the CBBT was designed and constructed in the early 1960s and first opened on April 15, 1964. The CBBT system consists of two tunnels, four artificial islands, and four bridges with lengthy causeways at both approaches as of 2020. Later expansions are expected to be carried out to increase the capacity of the tunnels and bridges, because CBBT becomes insufficient for growing demand these

days. To determine the design wave heights for maintenance, upgrade, and expansion, statistical analyses of long-term wave climates are needed. However, there is a lack of reliable long-term wave observations in Chesapeake Bay. Thus, an accurate forecast/hindcast of wave spectra and integral wave parameters must be carried out to fill the data gap.

In this study, we developed two composite ANN models for predicting bay and ocean waves at buoy station 44,087 using wind data from six NDBC stations sparsely located in the bay area, water level from a nearby NOAA tidal station, and offshore wave data from the NDBC buoy station 44,099 located out of the bay. Because of the close distance between the CBBT and the buoy station 44,087, the simulated integral wave parameters and wave spectra at this buoy station can represent the wave fields near the CBBT. Based on the directional spectral wave data from buoys 44,099 and 44,087, we partitioned the complex wave field into bay waves generated in the estuary and ocean waves generated in the Atlantic Ocean according to the wave directions. For bay wave predictions, the results show a high prediction skill for estimating H_{m_0} and wave direction, with the R2 values around 0.87 and 0.86, respectively. The modeling accuracy of T_p is slightly lower, but the R^2 and RMSE values can still reach 0.63 and 0.42 s, respectively. For ocean wave predictions, the composite deep neural networks provide satisfactory results for simulating both H_{m0} and T_p at the bay buoy 44,087, with the R² values around 0.90 and 0.72, respectively. Furthermore, the simulated wave spectra are in good agreement with measurements, with RSEM around 0.034 and 0.029 m²/Hz for bay and ocean waves, respectively. Overall, the model-data comparisons show that the developed data-driven models are able to predict integral wave parameters and wave energy density spectra for both bay and ocean waves. One application of the developed models is to hindcast the wave spectra at buoy 44,087 during the Halloween storm in 1991. Our composite ANN models hindcast that the maximum H_{m0} of ocean waves reached 1.4 m at bay buoy 44,087 during the Halloween storm, which is about

twice larger than that of bay waves. Moreover, model results show that the energy of ocean waves was much higher than that of bay waves, indicating that the wave energy near the CBBT mostly came from the Atlantic Ocean during the storm. However, because of the large fetch of Chesapeake Bay, bay waves generated by strong northwesterly wind could have wave height comparable to that of ocean waves at the study site, albeit much shorter wave periods and at a different time. This suggests that the bridge and tunnel system needs to consider waves generated from both the estuary and the ocean.

Overall, this study provides a novel framework for developing surrogate models to estimate wave spectra in the frequency domain and predict integral wave parameters, including H_{m0} , T_p , and Dir. The approaches shown in this study can be employed to provide fast estimations of wave spectra or downscaling of ocean wave model results when location-specific predictions are required, serving as a useful tool for the characterization and simulation of the wave environment. Note that the input features (e.g., wind and offshore waves) should be long enough so that the training data can be representative of the wave climates in different years. In closing, the information about the wave spectra and parameter estimates in this study can be useful for maintaining and expanding the CBBT system. Also, the novel framework for predicting wave spectra in the frequency domain and integral wave parameters can be applied to other coasts and estuaries.

CRediT authorship contribution statement

Nan Wang: Methodology, Software, Validation, Writing – original draft. Qin Chen: Conceptualization, Methodology, Investigation,

Writing – review & editing, Supervision, Funding acquisition. **Ling Zhu:** Investigation, Data curation, Writing – review & editing.

Declaration of Competing Interest

The authors declare that they have no known competing financial interests or personal relationships that could have appeared to influence the work reported in this paper.

Data availability

Data will be made available on request.

Acknowledgments

This paper is based upon work supported by the National Science Foundation under Award No. 2139882/2052443. Any opinions, findings and conclusions or recommendations expressed in this paper arethose of the authors and do not necessarily reflect the views of the National Science Foundation. Anyuse of trade, firm, or product names is for descriptive purposes only and does not imply endorsementby the U. S. Government.

Appendix

The definitions of wave parameters applied in this study are as follows.

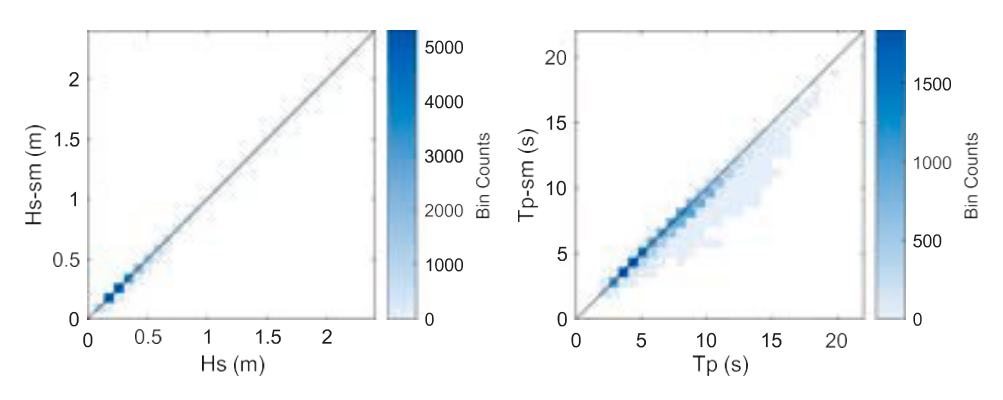


Fig. A1. Comparison between the wave parameters derived from the original frequency spectra and smoothed spectra at buoy 44,087.

Table A1List of wave parameters used in this study.

Parameter	Definition
H_{m0}	$H_{\rm m0} = 4\sqrt[4]{m_0}$
	m_n is the n^{th} moment of the frequency wave spectrum (Sverdrup and Munk, 1947), calculated as $m_n = \int_0^\infty f^n E(f) df$, where E is the spectral energy density in the frequency
	domain and f is the discretized frequency.
$T_{ m p}$	Period corresponding to the peak spectral frequency, f_p $f_p = \int_{1}^{\infty} \frac{f(E_f)^5 df}{\int_{1}^{\infty} [E(f)]^5 df}$ which reduces the errors associated with the estimate of f_p from the spectrum which is evaluated only at discrete values of frequency (Young and Verhagen, 1996).
Dir	Mean direction from which energy is coming at the peak period.
E_{max}	Maximum spectral energy density in the frequency domain.
S_{width}	The narrowness of the spectrum
	$S_{width} = \frac{1}{T_{m,0,2}} \frac{1}{T_{m,-1,0}} \frac{1}{1} \frac{1}{T_{m,0,2}} \frac{1}{T_$

Table A2
Statistical measures used in this study to evaluate the performance of the developed models.

MSE:	$MSE = \frac{\sum_{i} (y_i - \hat{y}_i)^2}{N}$ $\equiv = \frac{N}{N}$
RMSE:	$RMSE = \frac{1}{2} \sum_{k=1}^{\infty} \frac{1}{N}$
SI:	$SI = \frac{RMSE}{\overline{y}}$
bias:	$bias = \underbrace{\frac{1}{N}}_{N} \hat{y} - y$
R ² :	$bias = \sqrt{\frac{\sum_{i=1}^{N} \sum_{i} y_{i} - y_{i}}{\sum_{i} y_{i} - y_{i}}^{2}}}$ $R^{2} = \sqrt{\frac{\sum_{i} \sum_{i} y_{i} - y_{i}}{(y_{i} - y_{i})^{2}}^{2}}} (y_{i} - y_{i})^{2}$
Normalized SI performance:	SI = 1 - SI
Normalized bias performance:	$Bias = 1 - \frac{abs(bias)}{\overline{y}}$
Composite Performance Score:	$CPS = \frac{R^2 + 5I_{+} \circ bias}{3}$
Total composite performance score:	$TCPS = \frac{1}{3}(CPS_E + CPS_H + CPS_T)$

in which N is the number of samples, y_i is the estimated values, and y_i is the true value.

References

- Bai, G., Wang, Z., Zhu, X., Feng, Y., 2022. Development of a 2-D deep learning regional wave field forecast model based on convolutional neural network and the application in South China Sea. Appl. Ocean Res. 118, 103012.
- Basco, D., 2020. Design of Coastal Hazard Mitigation Alternatives For Rising Seas. World Scientific
- Bento, P.M.R., Pombo, J.A.N., Mendes, R.P.G., Calado, M.R.A., Mariano, S., 2021. Ocean wave energy forecasting using optimised deep learning neural networks. Ocean Eng. 219, 108372
- Booij, N., Ris, R.C., Holthuijsen, L.H., 1999. A third-generation wave model for coastal regions: 1. Model description and validation. J. Geophys. Res. Ocean. 104, 7649–7666
- Callens, A., Morichon, D., Abadie, S., Delpey, M., Liquet, B., 2020. Using Random forest and Gradient boosting trees to improve wave forecast at a specific location. Appl. Ocean Res. 104, 102339.
- Christakos, K., Gao, Z., Furevik, B.R., Bjo rkqvist, J.-.V., Aarnes, O.J., 2022. situ coastal observations of wave homogeneity and coherence. Appl. Ocean Res. 129, 103390.
- Cornejo-Bueno, L., Nieto-Borge, J.C., García-Díaz, P., Rodríguez, G., Salcedo-Sanz, S., 2016. Significant wave height and energy flux prediction for marine energy applications: a grouping genetic algorithm - Extreme Learning Machine approach. Renew. Energy 97. https://doi.org/10.1016/j.renene.2016.05.094.
- Dabbi, E.P., Haigh, I.D., Lambkin, D., Hernon, J., Williams, J.J., Nicholls, R.J., 2015. Beyond significant wave height: a new approach for validating spectral wave models. Coast. Eng. 100, 11–25.
- Deo, M.C., Naidu, C.S., 1998. Real time wave forecasting using neural networks. Ocean Eng 26, 191–203.
- Designing buildings, 2020. Chesapeake Bay Bridge-Tunnel [WWW Document]. URL. https://www.designingbuildings.co.uk/wiki/Chesapeake_Bay_Bridge-Tunnel.
- DHI, M., 2017. MIKE 21 Spectral Wave Module, Scientific Documentation. DHI Water Environ. Heal, Hørsholm, Denmark.
- Earle, M.D., Steele, K.E., Wang, D.W.C., 1999. Use of advanced directional wave spectra analysis methods. Ocean Eng. 26, 1421–1434.
- Elbisy, M.S., Elbisy, A.M.S., 2021. Prediction of significant wave height by artificial neural networks and multiple additive regression trees. Ocean Eng. 230, 109077.
- Hanson, J.L., Phillips, O.M., 2001. Automated analysis of ocean surface directional wave spectra. J. Atmos. Ocean. Technol. 18, 277–293.
- Huang, L., Jing, Y., Chen, H., Zhang, L., Liu, Y., 2022. A regional wind wave prediction surrogate model based on CNN deep learning network. Appl. Ocean Res. 126, 103287.

- James, S.C., Zhang, Y., O'Donncha, F., 2018. A machine learning framework to forecast wave conditions. Coast. Eng. 137 https://doi.org/10.1016/j. coastaleng.2018.03.004.
- Jo"rges, C., Berkenbrink, C., Stumpe, B., 2021. Prediction and reconstruction of ocean wave heights based on bathymetric data using LSTM neural networks. Ocean Eng. 232, 109046.
- Karimpour, A., Chen, Q., Twilley, R.R., 2017. Wind wave behavior in fetch and depth limited estuaries. Sci. Rep. 7, 40654.
- Lee, J.-.W., Irish, J.L., Bensi, M.T., Marcy, D.C., 2021. Rapid prediction of peak storm surge from tropical cyclone track time series using machine learning. Coast. Eng. 170, 104024.
- Mariotti, G., Huang, H., Xue, Z., Li, B., Justic, D., Zang, Z., 2018. Biased wind measurements in estuarine waters. J. Geophys. Res. Ocean. 123, 3577–3587.
- Miky, Y., Kaloop, M.R., Elnabwy, M.T., Baik, A., Alshouny, A., 2021. A Recurrent-Cascade-Neural network-nonlinear autoregressive networks with exogenous inputs (NARX) approach for long-term time-series prediction of wave height based on wave characteristics measurements. Ocean Eng 240, 109958.
- Mohaghegh, F., Murthy, J., Alam, M.-.R., 2021. Rapid phase-resolved prediction of nonlinear dispersive waves using machine learning. Appl. Ocean Res. 117, 102920.
- Namekar, S., Deo, M.C., 2006. Application of artificial neural network model in estimation of wave spectra. J. Waterw. Port, Coastal, Ocean Eng. 132, 415–418.
- Oh, J., Suh, K.-.D., 2018. Real-time forecasting of wave heights using EOF-wavelet-neural network hybrid model. Ocean Eng 150, 48-59.
- Rogers, W.E., Van Vledder, G.P., 2013. Frequency width in predictions of windsea spectra and the role of the nonlinear solver. Ocean Model 70, 52–61.
- Sadeghifar, T., Nouri Motlagh, M., Torabi Azad, M., Mohammad Mahdizadeh, M., 2017.
 Coastal wave height prediction using recurrent neural networks (RNNs) in the South Caspian Sea. Mar. Geod. 40. https://doi.org/10.1080/01490419.2017.1359220.
- Saha, S., Moorthi, S., Pan, H.-.L., Wu, X., Wang, Jie, Nadiga, S., Tripp, P., Kistler, R., Woollen, J., Behringer, D., Liu, H., Stokes, D., Grumbine, R., Gayno, G., Wang, Jun, Hou, Y.-.T., Chuang, H.-.Y., Juang, H.-M.H., Sela, J., Iredell, M., Treadon, R., Kleist, D., Delst, P., Van, Keyser, D., Derber, J., Ek, M., Meng, J., Wei, H., Yang, R., Lord, S., van den Dool, H., Kumar, A., Wang, W., Long, C., Chelliah, M., Xue, Y., Huang, B., Schemm, J.-.K., Ebisuzaki, W., Lin, R., Xie, P., Chen, M., Zhou, S., Higgins, W., Zou, C.-.Z., Liu, Q., Chen, Y., Han, Y., Cucurull, L., Reynolds, R.W., Rutledge, G., Goldberg, M., 2010a. NCEP Climate Forecast System Reanalysis (CFSR) Selected Hourly Time-Series Products. January 1979 to December 2010.
- Saha, S., Moorthi, S., Pan, H.-.L., Wu, X., Wang, J., Nadiga, S., Tripp, P., Kistler, R., Woollen, J., Behringer, D., 2010b. The NCEP climate forecast system reanalysis. Bull. Am. Meteorol. Soc. 91, 1015–1058.
- Saha, S., Moorthi, S., Wu, X., Wang, J., Nadiga, S., Tripp, P., Behringer, D., Hou, Y.-T., Chuang, H., Iredell, M., 2014. The NCEP climate forecast system version 2. J. Clim. 27, 2185–2208.
- Sakhare, S., Deo, M.C., 2009. Derivation of wave spectrum using data driven methods. Mar. Struct. 22, 594-609.
- Song, Y., Jiang, H., 2022. In: An Empirical Spectral Wave Model Based on Deep Learning, in: International Ocean and Polar Engineering Conference.
- Stringari, C.E., Harris, D.L., Power, H.E., 2019. A novel machine learning algorithm for tracking remotely sensed waves in the surf zone. Coast. Eng. 147, 149–158.
- Tang, T., Adcock, T.A.A., 2021. Data driven analysis on the extreme wave statistics over an area. Appl. Ocean Res. 115, 102809.
- Ti, Z., Song, Y., Deng, X., 2022. Spatial-temporal wave height forecast using deep learning and public reanalysis dataset. Appl. Energy 326, 120027.
- Tolman, H.L., 2009. User manual and system documentation of WAVEWATCH III TM version 3.14. Tech. note. MMAB Contrib. 276.
- Wang, N., Chen, Q., Chen, Z., 2022a. Reconstruction of nearshore wave fields based on physics-informed neural networks. Coast. Eng, 104167.
- Wang, N., Chen, Q., Zhu, L., Sun, H., 2022b. Integration of data-driven and physics-based modeling of wind waves in a shallow estuary. Ocean Model. 101978. https://doi. org/10.1016/j.ocemod.2022.101978.
- Wang, N., Chen, Q., Zhu, L., Wang, H., 2022c. Data-driven modeling of wind waves in upper Delaware Bay with living shorelines. Ocean Eng. 257, 111669 https://doi.org/ 10.1016/j.oceaneng.2022.111669.
- Wei, Z., 2021. Forecasting wind waves in the US Atlantic Coast using an artificial neural network model: towards an AI-based storm forecast system. Ocean Eng. 237, 100646.
- Wei, Z., Davison, A., 2022. A convolutional neural network based model to predict nearshore waves and hydrodynamics. Coast. Eng. 171, 104044.
- Yagci, O., Kitsikoudis, V., 2015. Machine learning based mapping of the wave attenuation mechanism of an inclined thin plate. Appl. Ocean Res. 53, 107-115.
- Zheng, Z., Ma, X., Ma, Y., Dong, G., 2020. Wave estimation within a port using a fully nonlinear Boussinesq wave model and artificial neural networks. Ocean Eng. 216, 108073.